Chapter 5

Improved Efficiency Silicon Wire Array Solar Cells

5.1 Abstract

In response to the work completed in Chapter 4, further studies of silicon wire arrays as photoelectrochemical solar cells were conducted. By using longer wires and optimizing the epoxy encapsulation, significantly improved short circuit current densities (J_{sc}) and fill factors were observed compared to previous results. Simultaneous with the improvement in J_{sc} and fill factor, a reduction in open circuit voltage (V_{oc}) was observed, but the overall energy conversion efficiency was still significantly improved over that observed in Chapter 4. Furthermore, verification that the photoactivity was due to the Si wires as opposed to the single-crystalline Si substrate was obtained by measuring the substrate after removal of the wires and by using scanning confocal microscopy to selectively excite the wires rather than the substrate. The observed energy conversion efficiencies can be significantly improved by correcting the raw data for both concentration overpotential losses and series resistance losses, and the validity of the concentration overpotential correction was verified by the use of a photoelectrochemical cell exhibiting significantly reduced concentration overpotentials. Finally etching of Si wires to remove the outer layers was preliminarily found to only decrease the observed efficiency, implying that further improvements in efficiency will require the use of different growth catalysts or improved methods for removing Au from the wires following growth.

5.2 Introduction

The results presented in Chapter 4 show that significant photovoltages are obtainable from silicon wire array samples produced by chemical vapor deposition (CVD) from Au catalyst particles.[1] However, in order to achieve significant energy conversion efficiencies, it will be necessary to demonstrate much higher currents and fill factors than those observed in the initial studies. For individual wires, simulations show that radial junction wires should be able to achieve nearly unity quantum efficiency across most of the Si absorption spectrum.[2] Thus the studies presented in this chapter have focused on measuring the *J-E* curves of wires that are significantly longer than those considered in Chapter 4, and on understanding the contributions of the substrate and the surface treatment of the wires on the observed values of V_{oc}, J_{sc}, fill factor, and efficiency.

5.2.1 CVD Grown Silicon Wires

Growth of silicon wire arrays by chemical vapor deposition (CVD) is a promising route to the inexpensive, scalable synthesis of structured silicon devices starting from widely available starting materials. CVD by the vapor-liquid-solid (VLS) method to grow Si wires was pioneered by Wagner and Ellis in the 1960s (Figure 5.1).[3] Since then, many studies have shown the controlled synthesis of silicon wires of many different sizes by using the CVD-VLS mechanism with Au catalyst particles.[4-15] In addition to CVD,

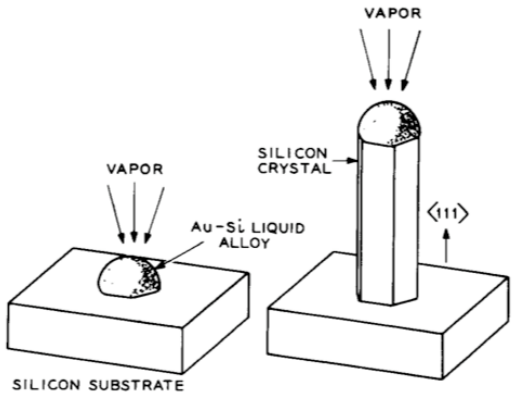

Figure 5.1. *Schematic of the VLS growth mechanism.[3] Si precursor in the gas phase impinges on the catalyst particle, where it is dissolved and then precipitated, growing the Si wire.*

wirelike structures have also been etched into the surface of single-crystalline silicon samples by chemical means,[16-20] but CVD growth does not necessarily consume an expensive single crystalline substrate wafer and is therefore preferable from a cost perspective.

Work in the Atwater and Lewis groups has demonstrated controlled growth of uniform arrays of Si wires starting from either Au or Cu catalyst particles with $SiCl_4$ as the feed gas.[21] Uniform arrays are obtained by patterning the catalyst particles inside an oxide mask to prevent pooling of the metal at the high growth temperatures.[21] In the interest of conserving the expensive substrate Si wafers used during growth, removal of the arrays after embedding in polymers (e.g., polydimethylsiloxane—PDMS) was demonstrated, as was reuse of the underlying substrate following wire removal.[22,23] In addition, single wires grown in this way have been characterized in both 2- and 4-probe geometries to determine their resistivity, and individual wires with axial contacts have been measured as microscale solar cells.[24]

Although other growth catalysts are possible, the wire arrays examined in this study were all catalyzed by Au particles. Au is expected to form a deep level trap in Si,[25] and its equilibrium concentration at the growth temperature is roughly 10^{16} cm^{-3}.[26-28] This expected concentration was confirmed by secondary ion mass spectrometry (SIMS) experiments which showed a concentration in the bulk of about 10^{16} cm^{-3}, but a concentration in the 100 nm closest to the surface of around 10^{17}-10^{18} cm^{-3}.[29] At this bulk Au concentration, for a midgap trap state in n-type Si, the expected minority carrier lifetime in the bulk is given by:[25]

$$\tau_p = \frac{1}{\sigma_p v_{th} N_T} \tag{5.1}$$

where τ_p is the minority carrier lifetime, σ_p is the trap capture cross section, v_{th} is the thermal velocity, and N_T is the concentration of traps. Using the geometric cross section of a Au atom (~10^{-15} cm^2) and the thermal velocity in Si (~10^7 cm s^{-1}) with a concentration of 10^{16} cm^{-3} yields a lifetime of about 10 ns. To convert this to a minority carrier diffusion length, we use the hole diffusion coefficient in Si (~10 cm^2 s^{-1}):[25]

$$L_p = \sqrt{D_p \tau} \tag{5.2}$$

This gives a value of around 3 μm for the minority carrier diffusion length. Using single wire devices, the diffusion length in VLS grown wires was measured by scanning photomicroscopy and found to be around 2-2.5 μm. Thus, the minority carrier diffusion length is expected to be larger than the radius of these wires, so that all photogenerated minority carriers are expected to be collected by the radial junction.[2]

Another important consideration for Au-catalyzed wires is the potential for Au to increase the resistivity of the wires. It was found that increasing the Au concentration significantly above the dopant concentration in n-type Si could lead to an increase in resistivity of many orders of magnitude.[26] In this case, 2- and 4-probe measurements showed the wires to have relatively low resistivity as grown (~0.05 Ω-cm) indicating that no such process is occurring.[24] However, the mechanism of n-type doping is unknown, and early studies of the resistivity of Au-catalyzed wires showed significant batch-to-batch variability in resistivity. Furthermore, the wires used in most of these studies were

grown with higher purity Au catalyst and were typically found to have lower conductivity than those reported in the literature (M. Kelzenberg, personal communication, 2008).

5.2.2 Photoelectrochemistry

As in the preceding chapters, photoelectrochemical characterization of the CVD-grown wire arrays was primarily accomplished using the 1,1'-dimethylferrocene$^{+/0}$/ methanol system ($Me_2Fc^{+/0}$/methanol). This system has been used with great success in the past for characterization of Si as the absorber for solar energy conversion and has been well studied.[30-37] Solar energy conversion efficiencies with single crystalline silicon were in the range of 10-14%,[38-40] and multicrystalline silicon efficiencies exceeded 7%.[41] The surface properties of Si samples immersed in this medium are also known to be favorable, with low SRV values and high barrier heights.[30,42,43] This system is therefore ideal for making high barrier height conformal junctions to the wires grown by the CVD method.

5.2.3 Wire Arrays for Solar Energy

Semiconductor wire arrays have been used in the literature for a number of solar energy conversion endeavors. In particular, there has been significant work on the use of metal oxide wires in a dye-sensitized solar cell (DSSC) configuration,[44-47] although a number of studies have also used metal oxide nanowires as charge collectors in hybrid organic/inorganic solar cells.[48-50] In addition, silicon wires have also been used to change the reflectivity properties of silicon solar cells, in a manner comparable to that discussed in Section 3.2 for porous Si.[51] In these efforts, the semiconductor is not typically acting as the primary absorber, but is only present as a charge collector or as an optical element.

In addition, photoelectrochemical studies similar to those described in this chapter have been carried out on arrays of Si nanowires produced from porous alumina templates, and a significant shift in cyclic voltammetric peaks was observed at these wire arrays, indicating a photovoltage of about 200 mV.[52] Furthermore, a recent study has also explored the use of Si wire arrays produced by etching in a photoelectrochemical cell,[53] and there have been several recent reports of solid state junctions with Si nanowire arrays produced both by CVD-VLS[54,55] and by chemical etching.[56] Thus, there is significant precedent for the use of wire arrays in solar energy conversion, but the challenge remains to show efficient energy conversion *J-E* curves from semiconductor wire arrays used as the absorbing material.

5.3 Experimental

5.3.1 Reagents

Methanol (BakerDry, Baker, Phillipsburg, NJ), 49% (27 M) HF(aq) (Transene, Danvers, MA), and buffered HF(aq) (Transene) were used without further purification. Water (18 MΩ cm resistivity) was obtained from a Barnstead Nanopure system. Lithium perchlorate, $LiClO_4$ (Sigma-Aldrich), was fused under vacuum and stored under an inert atmosphere until use. Dimethylferrocene (Me_2Fc, Sigma-Aldrich) was sublimed at ~45 ºC under vacuum and was stored under an inert atmosphere until use. Dimethylferrocenium tetrafluoroborate (Me_2FcBF_4) was synthesized from Me_2Fc by addition of excess HBF_4 (Alfa Aesar, Ward Hill, MA) in the presence of 0.5 equivalents of benzoquinone (Sigma-Aldrich). The reaction was conducted in an ice-water bath. The

resulting solid was dried under vacuum and stored in an inert atmosphere. Me_2Fc and Me_2FcBF_4 were stored in light-protected bottles.

Silicon (Czochralski, n-type, (100)-oriented, P-doped) for use as the planar electrode in studies employing high [Me_2Fc^+] was obtained from Wacker Siltronic (Munich, Germany, 4-8 Ω cm resistivity). These wafers were 500 ± 25 μm thick, polished on one side, and had measured resistivities between 5 and 7 Ω-cm.

5.3.2 Fabrication of Wire Array Samples and Controls

Degenerately doped N-type Si(111) wafers (0.004 Ω-cm) were thermally oxidized to produce a 285 nm oxide film. These wafers were then coated with S1813 photoresist (Microchem, Newton, MA), exposed to the pattern (square array of 3 μm holes, 7 μm center to center), and developed in MF319 (Microchem). The wafers were then etched for 4 min in buffered-HF improved (Transene), followed by thermal evaporation of 500 nm gold (99.9999%) and lift-off of the photoresist, to leave the catalyst islands separated by an oxide buffer. The samples were then brought into a tube furnace at 1050°C and annealed in H_2 for 20 min at a flow rate of 1000 sccm. The wires were subsequently grown in a mixture of H_2 (1000 sccm) and $SiCl_4$ (20 sccm) in order to produce wires of ~100 μm length (about 30 minutes).

5.3.3 Electrode Preparation and Treatment

Following growth, the wire array samples were etched for 10 s in buffered HF to remove the native oxide. The samples were then soaked for 45 min in TFA solution (Transene), which contains I^-/I_3^-, to etch away the gold particles. SEM images confirmed removal of the bulk of the Au catalyst particle (See Figure 5.3). The wire array samples were subsequently dipped in 1 M HCl(aq) and rinsed with H_2O. The samples were then

etched for 10 s in buffered HF to remove native oxide, rinsed with H_2O, and dried under a stream of N_2. Ga/In was immediately rubbed onto the back of the sample, and the samples were attached to a wire coil using silver paint. The samples were then sealed inside a glass tube, leaving 2-4 mm^2 of exposed front surface area, using Hysol 9460 epoxy (Loctite) to coat the front face and sealing the rest of the sample with Hysol 1C epoxy (Loctite). Hysol 9460 is used on the front face because it does not wick into the wire array to an appreciable extent.

For physical removal of wires from the substrate, the corner of a borosilicate glass slide was used to gently scrape the wires away from the surface, followed by a cotton swab soaked in methanol. Very little force was necessary to remove the wires, and the resulting surface typically regained a reflective sheen. For chemical wire etching, a 30% (w/w) solution of KOH in H_2O was used at room temperature with agitation or stirring. Following each etching step in KOH, the electrodes were rinsed with water/methanol/ acetone/methanol/water and etched again for 10 s in buffered HF to remove any oxide that formed during the etching procedure.

For scanning confocal microscopy studies, the Au catalyst was first removed from a large area wire array as described above. The array was then subsequently etched 10 s in buffered HF to remove the native oxide and affixed to a copper mount using Ga/In eutectic followed by silver paint. The cell for confocal microscopy experiments was then assembled under an inert atmosphere.

5.3.4 Photoelectrochemical Measurements

Under white light, the photoelectrochemical measurements were performed in a solution consisting of 200 mM of 1,1'-dimethylferrocene (Me_2Fc), 0.5 mM of Me_2FcBF_4, and 1 M of $LiClO_4$ in methanol. Methanol was clearly observed to wet the wire array surfaces during both processing and photoelectrochemical measurements. The working electrode was a wire array sample. The counter electrode was a Pt mesh, and the reference electrode was a Pt wire enclosed in a Luggin capillary that contained the same solution as the main cell. All cell components were assembled under an inert atmosphere and were sealed before being placed under positive pressure of Ar. During measurements, the cell was illuminated using a 300 W ELH-type projector bulb with a dichroic rear reflector.[57] The light intensity was calibrated using a Si photodiode to produce a photocurrent equivalent to that obtained under 100 mW cm^{-2} of AM 1.5 illumination at the working electrode surface. For Si photoelectrodes in this same cell configuration and electrolyte/redox system, this calibration method has been shown previously to produce short-circuit photocurrent densities that are very close to those obtained under the same intensity of actual sunlight.[39,40] The solution was stirred vigorously during measurement, and a stream of air was used to keep the cell temperature constant under illumination.

All current density-potential (*J-E*) measurements were recorded using a Solartron model 1287 potentiostat. In a typical experiment, the *J-E* behavior of the electrode was measured at 5 mV s^{-1} in the dark and then under 100 mW cm^{-2} of illumination. The open-circuit voltage, V_{oc}, was measured between each *J-E* measurement. The short-circuit

current density, J_{sc}, was calculated as the average current density for potentials within 10^{-4} V of 0 V versus the Nernstian potential of the cell. The values of V_{oc} and the presented *J-E* behavior are reported with respect to the Nernstian cell potential, which was measured with respect to the reference electrode for each working electrode. The Nernstian potential was typically 10-30 mV positive of the reference electrode potential, due to drift in the composition of the cell solution compared to the composition of the solution in the Luggin capillary. The point of maximum power was calculated as the average of 10 data points, after eliminating the 10 largest measured points (to remove any erroneous spikes). The efficiency and fill factor were calculated by conventional methods.

Photoelectrochemical experiments were also performed with an increased concentration of Me_2Fc^+ present. In this case, the solution consisted of 200 mM Me_2Fc, 50 mM Me_2FcBF_4, and 1 M $LiClO_4$ in methanol. All other procedures were identical to those described above except that monochromatic illumination was used due to the high absorption of Me_2Fc^+ in the visible. In this case, samples were illuminated with a diode laser emitting at 808 nm that had been passed through a diffuser to give uniform light intensity. The laser intensity was set for each measurement by matching the plateau current to the current measured for the same electrode under AM 1.5 in the cell having only 0.5 mM Me_2FcBF_4. In addition to the wire array samples tested, equivalent samples constructed from planar (100) Si samples were also tested with both small and large [Me_2Fc^+].

5.3.5 Correction for Series Resistance and Concentration Overpotential

Corrections for concentration overpotential and series resistance losses were performed according to equations (5.3) and (5.4):[58]

$$\eta_{conc} = \frac{k_B T}{nq}\left\{\ln\left(\frac{J_{l,a}}{-J_{l,c}}\right) - \ln\left(\frac{J_{l,a} - J}{J - J_{l,c}}\right)\right\} \tag{5.3}$$

$$E_{corr} = E_{meas} - iR_S - \eta_{conc} \tag{5.4}$$

where k_B is Boltzmann's constant, T is the absolute temperature, q is the charge on an electron, n is the number of electrons transferred in the redox process (n = 1 for $Me_2Fc^{+/0}$), $J_{l,c}$ and $J_{l,a}$ are the cathodic and anodic limiting current densities, respectively, and R_s is the series resistance. The limiting cathodic and anodic current densities were determined by use of a Pt foil working electrode in the same geometry as the Si working electrode, in contact with the same electrolyte solution, and in the same cell configuration. For experiments in solutions with small [Me_2Fc^+], $J_{l,c}$ and $J_{l,a}$ were found to be -0.1 mA cm^{-2} and 60 mA cm^{-2}, respectively. When large [Me_2Fc^+] was used, $J_{l,c}$ was found to increase to -9.7 mA cm^{-2}. The series resistance was calculated by using equation (5.3) to correct the *J-E* data obtained using the Pt electrode for concentration overpotential losses. The inverse of the slope of the linear portion of the resulting *J-E* data, around 0 V vs the cell potential, was then evaluated to produce a value for R_s. Although the series resistance varied from measurement to measurement, due primarily to small differences in the placement of the Luggin capillary, the value was typically in the range of 130-180 Ω. To minimize the possibility of overcorrection, a value of 100 Ω was chosen as the value of the series resistance used for the low [Me_2Fc^+] conditions.

This value should be an underestimate of the actual series resistance, particularly because the contact resistance and the series resistance of the silicon are not accounted for by the resistance data obtained using the platinum working electrode. Hence, the photoelectrode efficiencies calculated herein are conservative. For the cell with high [Me_2Fc^+], R_s was taken to be 150 Ω because an increased resistance was measured due to the difficulty of placing the Luggin capillary near the working electrode surface in the dark solution. Correction of the observed *J-E* behavior at the Si photoelectrodes for both series resistance and concentration overpotentials thus produced the values of E_{corr} reported herein for each measured potential, E_{meas}. When only one of the concentration overpotential or series resistance losses was corrected for, equation (5.4) was still used, but the appropriate term was dropped.

5.3.6 Diode Quality Factor Measurement

In order to measure the diode quality factor, electrodes were measured at a series of light intensities using the 808 nm diode laser in the cell with high [Me_2Fc^+]. At each light intensity the V_{oc} and the J_{sc} were measured using the Solartron 1287 potentiostat. The V_{oc} is expected to the have the general form:[59]

$$V_{oc} = \frac{AkT}{q} \ln\left(\frac{J_{ph}}{J_0}\right) = \frac{AkT}{q} \ln(J_{ph}) - \frac{AkT}{q} \ln(J_0) \tag{5.5}$$

where A is the diode quality factor, k is Boltzmann's constant, T is the temperature, q is the charge on an electron, J_{ph} is the photocurrent density, and J_0 is the dark saturation current density. Therefore, a plot of V_{oc} vs. J_{ph} should be linear with slope AkT/q, and the value of A can be readily extracted.

5.3.7 Scanning Confocal Microscopy Measurements

For scanning microscopy experiments, a silicon wire was affixed to a copper backing as described above. A flow cell was then assembled using an o-ring with three radial holes and a coverslip. Two of the radial holes allowed the cell to be filled through fluorocarbon turing with 50 mM Me_2Fc, 10 mM Me_2FcBF_4, and 1 M $LiClO_4$ in propylene carbonate under an inert atmosphere. The wire array electrode was connected to the virtual ground of a high-pass filtered transresistence preamplifier circuit. The counter electrode was connected to ground through a DC power supply. The preamplifier output was connected to a lock-in amplifier (Stanford Research), and the signal was measured from the lock-in amplifier output. The lock-in reference was provided by the optical chopper (Thorlabs) used to modulate the excitation beam. The sample was excited with a continuous wave 650 nm diode laser passed through the optical chopper operating at about 1 kHz and finally through a 20x long working distance microscope objective. The focused laser spot was then rastered across the sample and the photocurrent measured at each point as the output of the lock-in amplifier.

5.4 Results and Discussion

5.4.1 Wire Arrays

Vertically aligned arrays of high aspect ratio Si wires were produced by the CVD-VLS method using Au as the VLS catalyst.[21] In order to achieve good pattern fidelity, the substrate wafer is first patterned with an oxide buffer layer before Au deposition, which serves to prevent flow and pooling of the catalyst at the growth temperatures. Growth from wafers patterned in this way produces long, straight wires with the Au catalyst

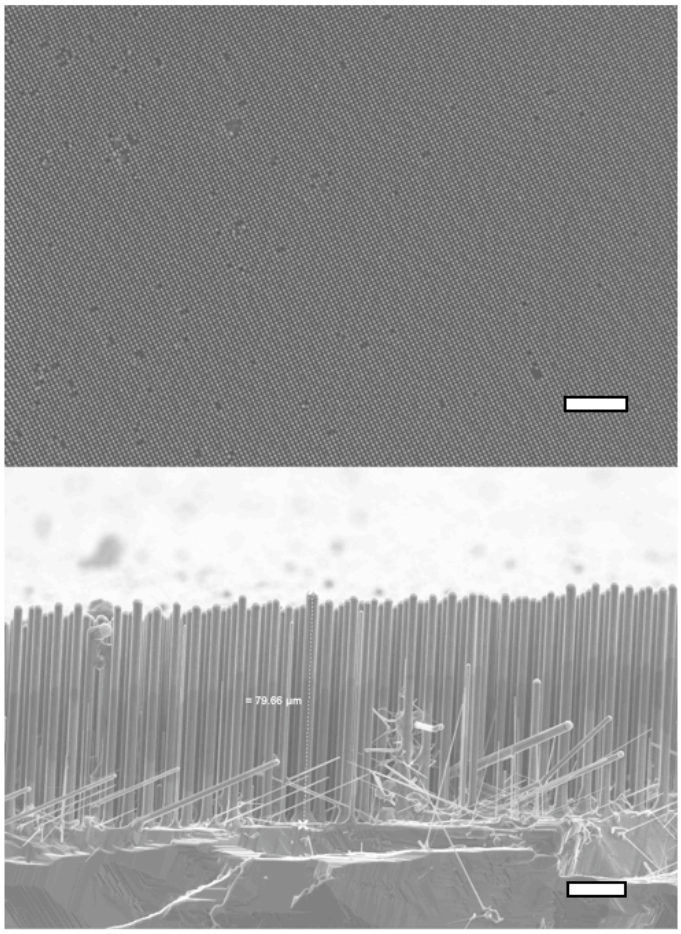

Figure 5.2. *Scanning electron micrographs of Si wire arrays. Top: Plan view showing the long range order in the arrays with some deletion defects. Scale bar, 100 µm. Bottom: Side view of the wires at the edge of the wafer. Some of the non-vertical wires are due to the growth at the sample edges. Scale bar, 20 µm.*

particle still clearly visible on the wire tip. The arrays shown in Figure 5.2 are representative of the samples used to obtain the photoelectrochemical results shown below. From the plan view of the wires, it is apparent that there are a significant number of deletion defects in the arrays, perhaps due to defects in the oxide or catalyst patterns resulting from the photolithography step. However, the cross-sectional image of the wires shows some nonvertical wire growth, and this may be another explanation for the observed defect density. It has been previously shown that wires produced under these conditions grow in the <111> direction,[21] and the angle between adjacent <111> vectors

is around 70º, which is approximately the angle observed between the vertically growing wires and those that grow at an angle. Thus, it is expected that the non-vertical wires are still growing in the <111> direction, but have developed a kink early in their growth.

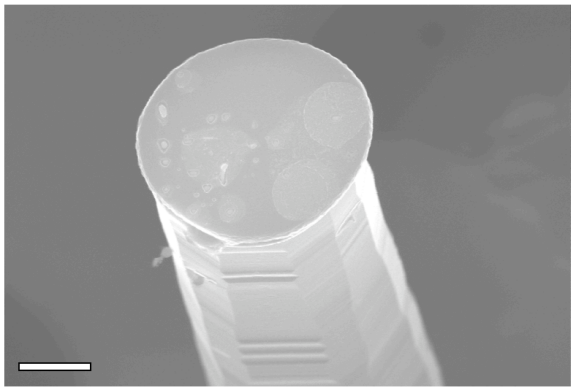

Figure 5.3. *Close up of the wire tip after removal of the catalyst particle. Note that the tip is flat and that the wire shows significant faceting. Scale bar 1 µm.*

The wires used in this study varied from ~80 to ~100 µm in length and typically had diameters of around 2-2.5 µm. This diameter is slightly smaller than the 3 µm diameter of the patterned catalyst particle, which is consistent with the significant taper typically observed at the very base of the wires. Following this initial taper, however, the wires grow with straight side walls, indicating that the catalyst particle does not shrink at a significant rate after growth initiation. Removal of the catalyst particle from the wires was accomplished using a proprietary etching solution containing I^-/I_3^-. Complete removal of the catalyst particles could be accomplished with this treatment, leaving a flat Si surface at the tips of the wires (Figure 5.3), although in some cases a thin, hollow shell of silicide was observed (not shown). The facets observed in Figure 5.3 are typically observed in the wires upon closer inspection, particularly following a short etch in KOH solution, which is an anisotropic etchant for Si.

5.4.2 Photoelectrochemical Performance

Photoelectrochemical measurements of wire array electrodes were carried out in a solution consisting of 1.0 M $LiClO_4$, 200 mM Me_2Fc, and ~0.5 mM Me_2FcBF_4 in methanol. This solution has been shown previously to give low surface recombination velocities and high open circuit potentials in contact with n-type Si.[30,42] Figure 5.4 shows representative *J-E* curves of wire array samples. Also shown in Figure 5.4 is the *J-E* characteristic of the substrate after the wires have been mechanically removed. We note that the J_{sc} is reduced by roughly one order of magnitude upon removal of the wires, indicating that the primary contribution to the photoactivity of the samples measured is due to the CVD-grown Si wires rather than the single crystalline Si substrate. This reduction in both photocurrent and photovoltage upon wire removal is consistently

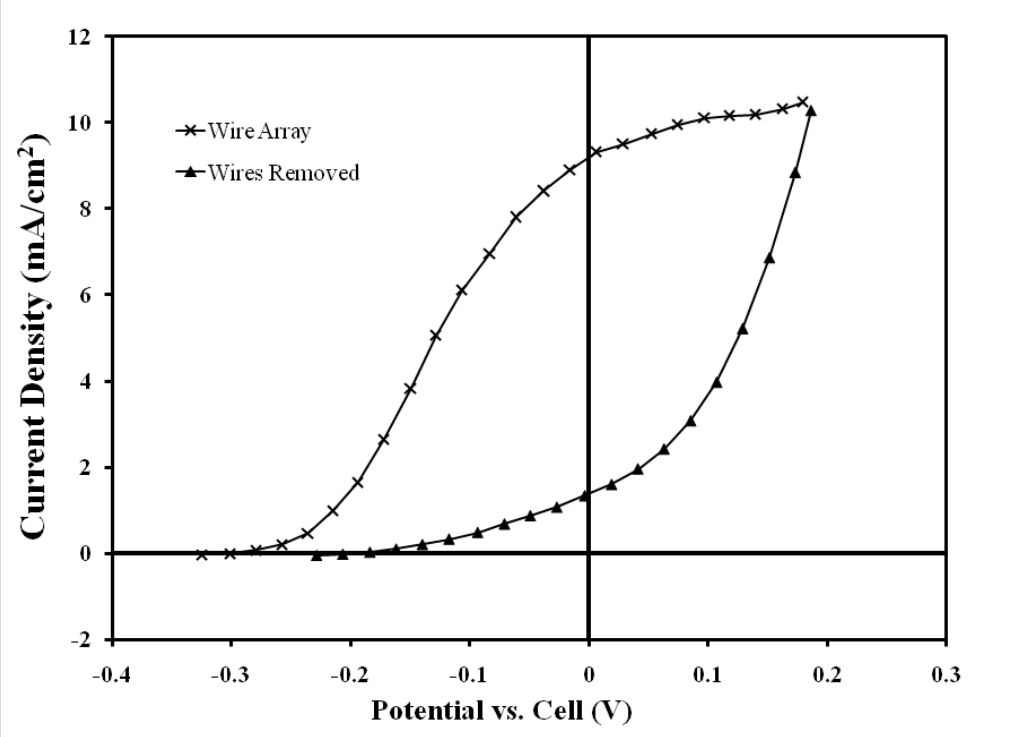

Figure 5.4. *Representative J-E curves for wire array electrodes and electrodes with the wires removed. The data is referenced to the Nernstian potential of the cell, and the scan rate was 5 mV/s.*

observed. This result is expected because the substrate wafer is heavily doped n^+-Si, which should therefore be nonphotoactive. Furthermore, the wire array growth is carried out in the presence of significant concentrations of Au, which has a relatively large diffusion coefficient at the growth temperatures employed (~10^{-6} cm^2 s^{-1} at 1050ºC).[27,28] Thus, we expect the contribution of the substrate to the observed photocurrent to be relatively minor and the remainder of this chapter will focus primarily on the behavior of the Si wires. For further evidence of the photoactivity of the wires over the substrate, see Section 5.4.5.

From the raw *J-E* curves, several features are immediately apparent. First, we note that the observed short circuit current density (~9 mA/cm^2) is significantly larger than the expected value based on the filling fraction of wires. Since the wires are patterned in a square array with 7 μm center-center distance and typically have diameters on the order of 2.5 μm, the filling fraction of Si in the wire layer is only about 10%. Given that the flux of incident energy in the AM 1.5 spectrum above the Si band gap gives rise to a maximum theoretical J_{sc} of ~43 mA/cm^2,[60] the 10% filling fraction of wires predicts a maximum observable J_{sc} of only 4.3 mA/cm^2. One possible explanation is that the lamp used is not exactly the same as AM 1.5, giving rise to artificially high photocurrents in Si. However, the results of Section 2.4.2 show that planar samples under the same illumination in the same cell show photocurrents of around 35 mA/cm^2, well less then the theoretical maximum.[61] Thus, the high J_{sc} implies significant light scattering within the wire array layer, leading to absorption of more light than just that incident directly on the tops of the wires. The optical absorption and scattering properties of the wire arrays have

been verified using arrays that have been embedded in polydimethylsiloxane (PDMS) and removed from the subsrate. Under these conditions, it was found that the wire array absorption was 2-3 times what would be expected from the simple filling fraction of the wires in the polymer (M. Kelzenberg, personal communication, 2008). Although the scattering in the Si wire/methanol system is expected to differ from that observed in the Si wire/PDMS system, the precedent for significant scattering based absorption of the wires, even at normal incidence, lends credence to the hypothesis that the observed values of J_{sc} are due primarily to the scattering of light.

In addition to the high currents observed from the raw data, the cathodic limiting current is also found to be very small (usually ~0.1 mA/cm^2). This is due to the much smaller concentration of Me_2FcBF_4 used in the cell as compared to the concentration of Me_2Fc. It is necessary to use only small amounts of Me_2Fc^+ when illuminating with white light because Me_2Fc^+ absorbs strongly in the visible, interfering with the penetration of light to the electrode surface. As discussed in Section 1.4.1, the small cathodic limiting current leads to a significant concentration overpotential loss, resulting in a significant reduction in fill factor. When the *J-E* curves are corrected for the concentration overpotential loss as described in the Section 5.3.5, the fill factor is noticeably improved (Figure 5.5). The anodic and cathodic limiting currents needed for the correction were obtained by measuring the *J-E* curve of a Pt electrode in the same cell and geometry as that used to measure the Si electrodes. The observed value of J_{sc} is also improved upon correction in these samples because the curves had not reached the plateau current before reaching short circuit due to the large potential shift from the

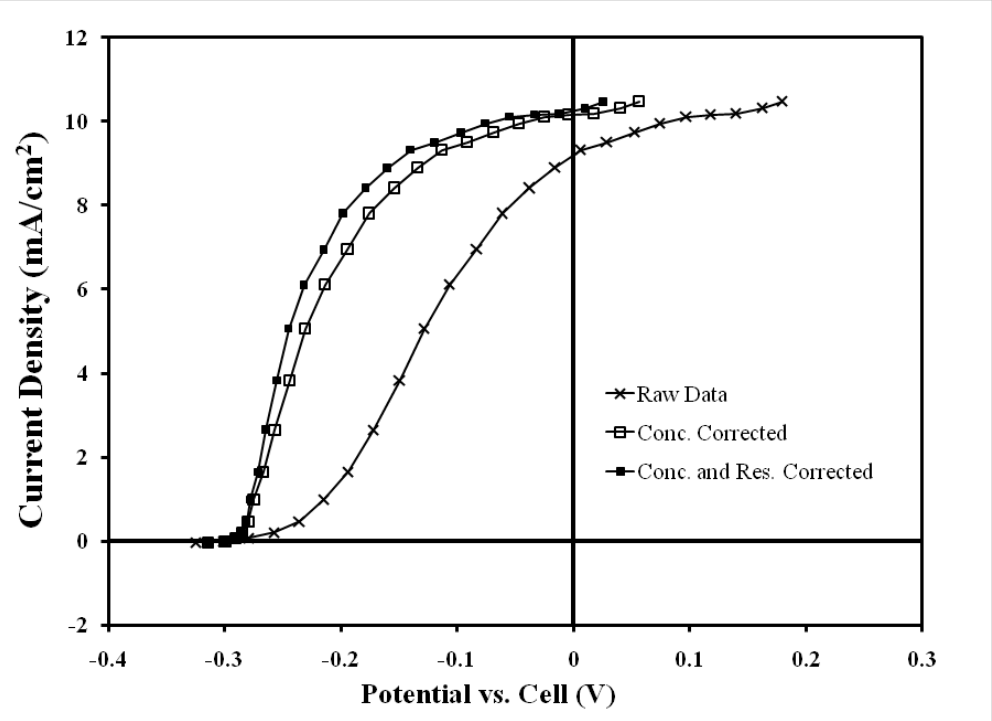

Figure 5.5. *Representative J-E curves for wire array electrodes after correction for concentration overpotential losses (Conc. Corrected) and both concentration overpotential and series resistance losses (Conc. and Res. Corrected).*

concentration overpotential loss. In addition to concentration overpotential loss, we also expect resistance losses due to the nonaqueous electrolyte. Even when using a Luggin capillary to reduce it, the solution series resistance is measured to be in excess of 100 Ω when using a Pt foil electrode in place of the Si working electrode. Further correction of the *J-E* curve for this series resistance leads to only a slight improvement in fill factor (Figure 5.5).

The observations made above by qualitatively examining representative *J-E* curves from wire array samples are supported quantitatively by the solar cell figures of merit observed for a set of wire array electrodes measured under the same conditions (Table 5.1). It is apparent from the change in fill factor that the contribution of the concentration overpotential loss is significantly larger than that of the solution series resistance loss.

Table 5.1. *Solar cell figures of merit for wire array electrodes grown from Au catalyst*

Data Correction[a]	J_{sc} (mA cm^{-2})[b]	V_{oc} (mV)[b]	Fill Factor (%)[b]	Efficiency (%)[b]
None	9.8 ± 0.4	262 ± 9	21 ± 1	0.55 ± 0.05
Conc. Only	11.7 ± 0.5	262 ± 9	44 ± 1	1.35 ± 0.08
Conc. and Res.	11.9 ± 0.5	262 ± 9	50 ± 2	1.56 ± 0.10

[a] Conc. Only indicates that only the concentration overpotential correction has been made, while Conc. and Res. indicate values extracted from J-E curves corrected for both concentration overpotential and series resistance.
[b] All values are the mean of eight independent samples, with the error given as the standard error of the mean.

Comparing these figures of merit with those found in Chapter 4,[1] we see that, while the J_{sc} has improved by nearly an order of magnitude, the V_{oc} has decreased by around 100 mV. The improvement in J_{sc} can be explained by several key changes from the samples examined in Chapter 4. First, it was stated in Chapter 4 that the wires were on the order of 20 μm in length, whereas the wires in this study are typically around 80-100 μm long. Furthermore, the epoxy used to encapsulate the samples examined in Chapter 4 was subsequently found to infiltrate the wire arrays to a significant extent, leaving only the tips of the wires exposed to solution. Since the wires generated are expected to have minority carrier diffusion lengths on the order of 2 μm,[24] leaving only the tips of the wires exposed will significantly reduce the collected current. Finally, the epoxy infiltrating the arrays in the samples from Chapter 4 was opaque, preventing the enhanced absorption due to scattering of light within the wire arrays. Thus, the wires in this study show much higher J_{sc} values because they are longer, have conformal contact along the full length of the wire, and have the possibility of enhanced absorption due to scattering.

We would also like to understand the observed V_{oc}, both in comparison with an ideal planar diode and in comparison to the results obtained in Chapter 4. In order to

understand the influence of geometrical affects on the observed V_{oc}, we can calculate the expected reduction in V_{oc} based on the increased surface area of the wires relative to a planar diode, given by (See Section 1.3.1):

$$V_{oc} = \frac{AkT}{q} \ln\left(\frac{I_{ph}}{\gamma I_0}\right) \tag{5.6}$$

From equation (5.6), it is apparent that the value of the diode quality factor, A, can be determined from the slope of a plot of V_{oc} vs. ln(I_{ph}). Performing this measurement gives an average value for the diode quality factor for the wire array samples examined here of ~1.6 (mean of 6 samples). We note that the observed diode quality factor for the wire arrays is significantly larger than 1, and that values of approximately 1.1 are obtained with photoactive planar samples under the same conditions. In all cases the plot of V_{oc} vs. ln(I_{ph}) was found to be linear with $R^2 > 0.999$. Thus, other recombination mechanisms besides bulk recombination ($A = 1$) are likely to be active in these devices, particularly depletion region recombination, which gives an expected diode quality factor of 2.[59] The simulations performed by Kayes et al. showed that depletion region recombination becomes quite important for devices with highly structured junctions,[2] so we expect to see significant contributions from depletion region recombination in these samples.

We calculate γ for equation (5.6) by assuming that all of the current collected is collected through the wire surface, not through the substrate (which is protected by a thick layer of oxide). In this case, we have:

$$\gamma = \frac{\text{wire surface area}}{\text{projected area}} \tag{5.7}$$

Therefore, we can easily calculate γ by taking the ratio of the wire surface area in one wire to the projected area of one unit cell. For 100 μm long wires with 2.5 μm diameter and 7 μm center-center distance in a square array, this gives $\gamma \approx 16$. Thus, we calculate a reduction in V_{oc} of only about 117 mV due to the increased junction area relative to a planar device. This value cannot account entirely for the poor V_{oc} measured for the wire arrays, and it suggests that the high concentration of Au in these wires is leading to a much reduced V_{oc} value due to recombination in the bulk and depletion regions in addition to the reduction from increasing γ.

Since the wires examined in Chapter 4 were also grown by Au-catalyzed CVD-VLS, we can compare the V_{oc} obtained in this study (262 mV) with the V_{oc} measured for those samples (389 mV).[1] As with the observed change in J_{sc}, geometrical concerns are again expected to play a significant role. For the shorter wires from Chapter 4, the decreased junction area relative to the projected area is expected to lead to an increased V_{oc} relative to the wire arrays examined here. Furthermore, we expect that carriers were collected primarily at the wire tips in the samples examined in Chapter 4 due to epoxy infiltration, thus further reducing the junction area and increasing the V_{oc} relative to the samples examined in this chapter. These effects combined lead to an increase in the effective surface area enhancement factor, γ, for the wires examined in this chapter relative to those studied in Chapter 4.

Assuming that the wires examined in Chapter 4 have a similar diode quality factor (~1.6), and taking into account the difference in photocurrents, it is possible to calculate the increase in γ that would be needed in order to account for the observed decrease in

V_{oc}. Based on this calculation, an increase in γ of more than a factor of 100 would been needed to fully explain the observed decrease in V_{oc}. Although γ is only ~16 for the long wires examined in this chapter, it is likely that the wires studied in Chapter 4 have an effective γ that is less than unity based on equation (5.7) because only a few microns of wire tip were exposed through the epoxy. Assuming 2 μm of wire were exposed in the samples from Chapter 4 gives a γ value of 0.42 for those wires, and thus a relative increase in γ by a factor of about 40 for the long wires considered here relative to the short, unintentionally encapsulated wires considered in Chapter 4. Although there is significant uncertainty in these calculations, they suggest that changes in γ due to geometrical changes cannot fully explain the observed decrease in V_{oc}. As another possible contributor to the change in V_{oc}, we expect to observe significant depletion region recombination in the long wires examined in this chapter, but much less in the wires examined in Chapter 4 since only the tips of the wires were exposed. This may lead to a smaller diode quality factor for the wires from Chapter 4, further enhancing the observed decrease in V_{oc}. Although a significant portion of the change in V_{oc} can be accounted for by geometrical effects, there may be significant differences in materials properties or doping levels giving rise to the observed difference in V_{oc}.

Finally, we note that the observed fill factor improves significantly upon correction for the concentration overpotential losses, leading to much improved efficiencies. These devices, although still not efficient enough for commercial use, are much more efficient than the devices studied in Chapter 4, largely due to the changes in geometry described above. Since the concentration overpotential has such a dramatic effect on the observed

fill factor and efficiency, further experiments were undertaken in order to verify that the fill factor and efficiency of the electrodes improve experimentally under relaxed concentration overpotential constraints.

5.4.3 Experimental Verification of *J-E* Curve Correction

In order to further probe the influence of the concentration overpotential loss, *J-E* curves were collected under conditions with an increased concentration of Me_2Fc^+ (50 mM instead of ~0.5 mM). Since the oxidized half of the redox couple absorbs strongly in the visible, it is necessary to use illumination of a wavelength where Me_2Fc^+ does not absorb strongly when using an appreciable concentration of Me_2Fc^+. Thus, for these experiments, the samples were illuminated with a diode laser emitting at around 808 nm. The laser intensity was set so that the plateau current under monochromatic illumination in high [Me_2Fc^+] was approximately equal to that observed under white light for the same electrode in the cell containing only ~0.5 mM Me_2Fc^+. Figure 5.6 shows representative *J-E* curves taken with high Me_2Fc^+ with various applied corrections for both planar (photoactive) and wire array samples. The photoactive planar samples have been included to demonstrate that the observed effect is not due to the wire array geometry. It is apparent from these plots that the corrections for both series resistance and concentration overpotential losses are much smaller under these conditions.

Representative *J-E* curves comparing small (~0.5 mM) and large (50 mM) [Me_2Fc^+] conditions for both planar and wire array samples are shown in Figure 5.7. For both planar and wire array samples, the improvement in the fill factor at the same J_{sc} and V_{oc} are clearly visible in the raw data. This is a direct manifestation of the concentration

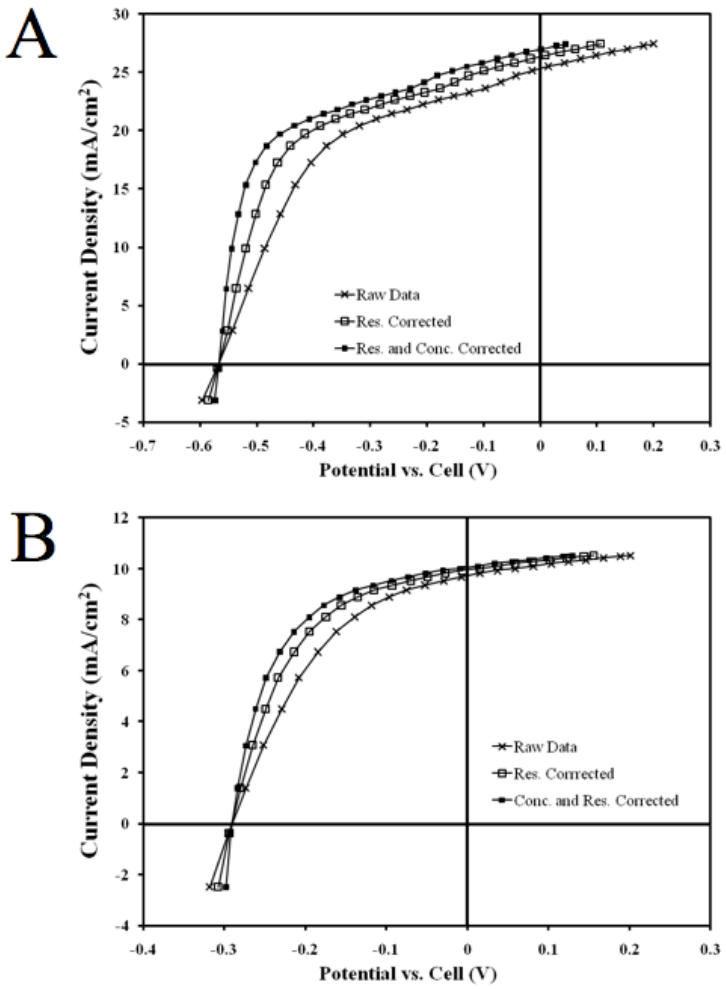

Figure 5.6. *Representative J-E curves collected with 200 mM Me_2Fc, 50 mM Me_2Fc^+, and 1.0 M $LiClO_4$ in methanol. Illumination was provided by an 808 nm diode laser with the intensity set to match the plateau current under AM 1.5 illumination. The scan rate was 5 mV/s. A) Planar, (100) sample corrected for resistance (Res.) or both resistance and concentration overpotential losses (Conc. and Res.). B) Wire array electrode.*

overpotential loss observed when the concentration of Me_2Fc^+ is much smaller. When monochromatic illumination was used in the cell with small [Me_2Fc^+], the *J-E* curves matched those obtained with white light when the laser intensity was adjusted to match the plateau currents (data not shown). Thus, the observed increase in fill factor is not due to the use of monochromatic illumination instead of white light and is a direct manifestation of the increased concentration of Me_2Fc^+.

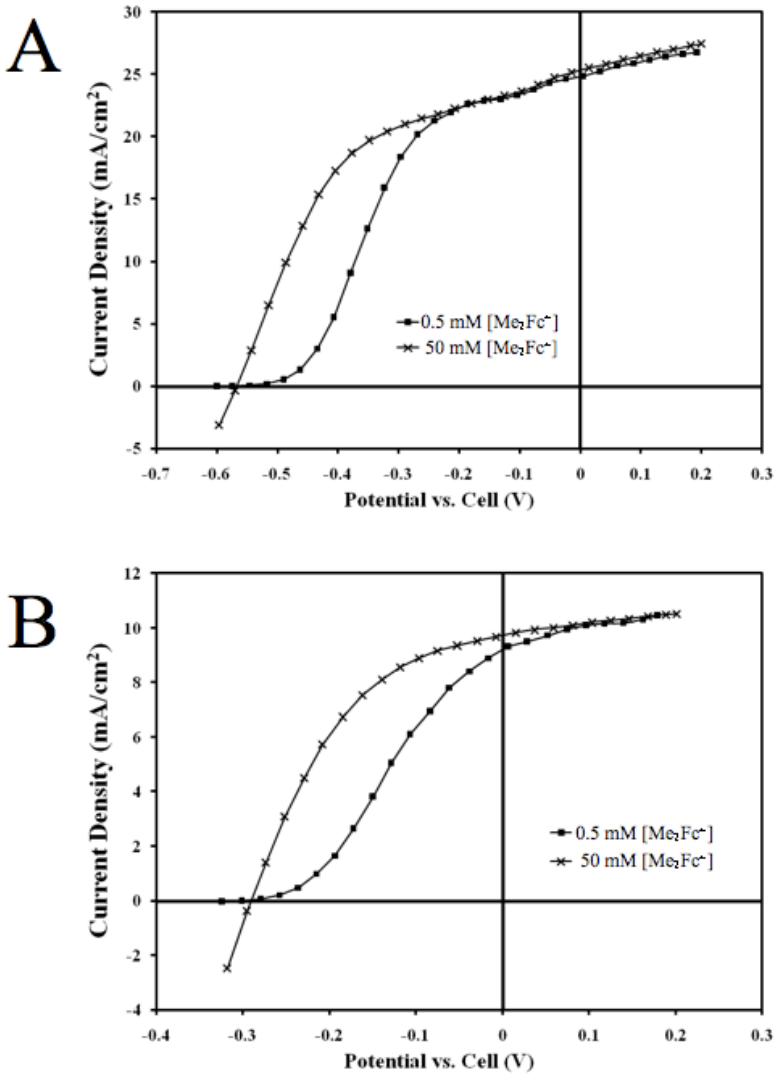

Figure 5.7. *Representative J-E curves comparing response in small [Me_2Fc+] and large [Me^2Fc+]. Samples were under AM 1.5 white light with small [Me_2Fc^+] or under 808 nm light with large [Me_2Fc^+], with the intensity set to match the plateau current at AM 1.5. A) Planar (100) Si sample. B) Wire array sample.*

Figure 5.8 (A and B) shows data collected with both small and large [Me_2Fc^+] when the concentration overpotential correction has been applied. The concentration overpotential corrected data from small [Me_2Fc^+] matches the raw data from large [Me_2Fc^+], as expected. However, even in the presence of 50 mM Me_2Fc^+, there is still a small but significant concentration overpotential loss. After making this correction to the 50 mM Me_2Fc^+ data, we see slightly better agreement between the two conditions for

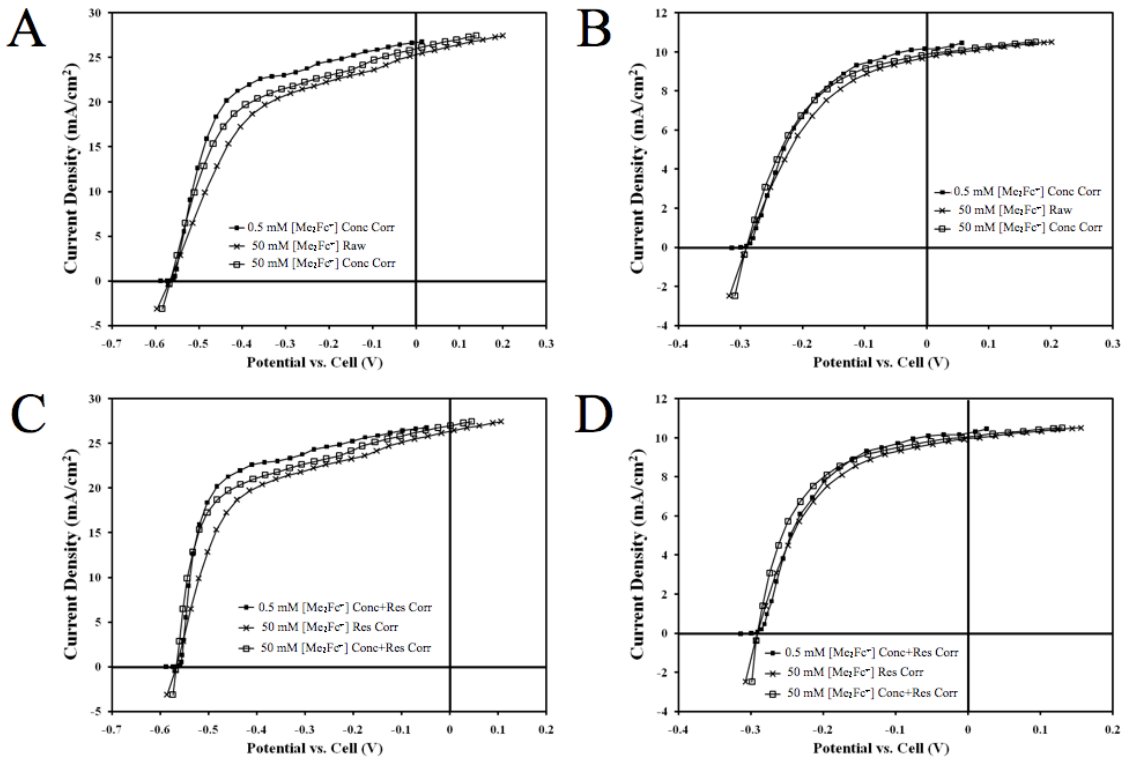

Figure 5.8. *Representative J-E curves with various corrections. As before, white light (AM 1.5) was used for 0.5 mM Me_2Fc^+, and 808 nm light was used for 50 mM Me_2Fc^+. A) Planar (100) samples, no resistance correction. B) Wire array samples, no resistance correction. C) Planar (100) samples, resistance corrected. D) Wire array samples, resistance corrected.*

both planar and wire array samples. This agreement is further evidence in support of the validity of the concentration overpotential correction.

The data shown in Figure 5.8 (C and D) have been corrected for series resistance losses. We also expect to observe agreement between *J-E* curves collected with large [Me_2Fc^+] that have been corrected for series resistance and *J-E* curves collected with small [Me_2Fc^+] that have been corrected for both concentration overpotential and series resistance losses. Figure 5.8 (C and D) supports this hypothesis, although a small correction for the remaining concentration overpotential loss with large [Me_2Fc^+] slightly improves the agreement in the planar case. Taken together, these data suggest that the

theoretically predicted correction for the concentration overpotential loss corresponds closely to the physical reality of the system.

The qualitative observations made above based on the representative *J-E* curves are corroborated by solar cell figures of merit obtained for a number of independent wire array electrodes (Table 5.2). As expected, the value of J_{sc} was approximately the same for all conditions and corrections with the exception of the raw data obtained with small [Me_2Fc^+]. In the latter case, many of the wire array samples had not reached the plateau current before short circuit due to large concentration overpotential losses. Neither the concentration overpotential correction nor the resistance loss correction affects the value of V_{oc}, so the only observed difference is between small [Me_2Fc^+] and large [Me_2Fc^+]. Although a slight drop in the average V_{oc} is observed upon changing to monochromatic illumination, this difference is not statistically significant. If there is a real difference in the V_{oc}, it could be due to the use of red light instead of white light, giving rise to more

Table 5.2. *Solar cell figures of merit for wire array samples measured with small and large [Me_2Fc^+]*

[Me_2Fc^+]	Data Correction[a]	J_{sc} (mA cm^{-2})[b]	V_{oc} (mV)[b]	Fill Factor (%)[b]
~0.5 mM	None	9.8 ± 0.6	254 ± 9	20 ± 1
~0.5 mM	Conc. Only	11.9 ± 0.6	254 ± 9	44 ± 2
~0.5 mM	Conc. and Res.	12.2 ± 0.7	254 ± 9	50 ± 2
50 mM	None	11.4 ± 0.7	249 ± 9	41 ± 1
50 mM	Res. Only	11.8 ± 0.8	249 ± 9	49 ± 1
50 mM	Conc. Only	11.7 ± 0.7	249 ± 9	46 ± 1
50 mM	Conc. and Res.	12.0 ± 0.8	249 ± 9	55 ± 1

[a] Samples have been corrected for concentration overpotential (Conc.) and solution series resistance (Res.) as indicated.
[b] Values reported are the mean of six independent electrodes and error values are the standard error of the mean.

uniform carrier generation in the wires and therefore more uniform flux across the junction (See Section 3.4.3), but the effect is very small in this case.

The most important parameter listed in Table 5.2 is the fill factor. We see that the fill factor is quite low for the raw data collected in small [Me_2Fc^+], but at least a factor of two higher for all the other entries in the table. In particular, we note that the fill factor for uncorrected data collected in large [Me_2Fc^+] is similar to the fill factor obtained when the data collected in small [Me_2Fc^+] is corrected only for concentration overpotential. As described above, correcting the data with large [Me_2Fc^+] for the remaining concentration overpotential loss under those conditions further improves the observed agreement with the concentration overpotential corrected small [Me_2Fc^+] data. Similarly, correcting the large [Me_2Fc^+] data for only series resistance losses gives a fill factor that is very similar to that obtained when the data collected with small [Me_2Fc^+] is corrected for both series resistance and concentration overpotential losses. Taken together, these data provide strong evidence that the concentration overpotential correction undertaken for small [Me_2Fc^+] is valid for this cell. Therefore, these experiments also validate the relatively high efficiencies obtained from the corrected data, implying that production of a cell that mitigates both concentration overpotential and series resistance losses would yield efficiencies on the order of 1.5% for these wire arrays.

5.4.4 Preliminary Wire Surface Removal Results

Impurity profiling experiments on wires grown by CVD-VLS from Au catalyst particles have shown that there is a Au rich layer near the surface of the wires.[29] As a result, etching of the wire surface using KOH was undertaken to explore the possibility of

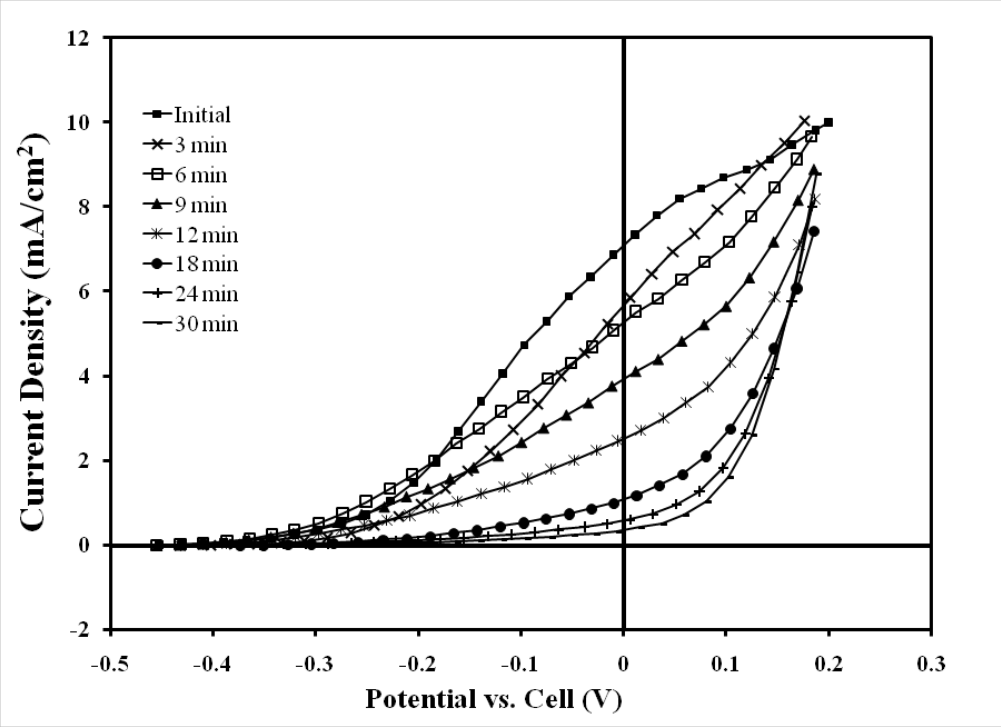

Figure 5.9. *J-E curves under AM 1.5 illumination in 200 mM Me_2Fc, 0.5 mM Me_2FcBF_4, and 1.0 M $LiClO_4$ in methanol. The scan rate was 5 mV/s. Etching was conducted in 30% KOH in water (w/w), and etch times are indicated in the legend.*

improving the wire performance by removing the near-surface Au rich layer. Figure 5.9 shows representative *J-E* curves for the etching of one wire array sample. Under the conditions used in this experiment, 3 min of etching in KOH should correspond to the removal of approximately 100 nm of Si from all exposed surfaces, or about a 200 nm reduction in diameter for each 3 minutes of etching.[62] It is apparent from Figure 5.9 that the primary effect of KOH etching is the reduction of J_{sc}. After etching for 30 min, it is expected that about 2 μm of wire diameter have been removed, corresponding to approximately the entire wire. Indeed, after 30 min of etching there is very little remaining photoresponse from the wire arrays. This observation further corroborates that the n^+-Si substrate is not photoactive following the growth procedure and that the *J-E* curves collected primarily reflect the photoactivity of the wires rather than the substrate.

The results shown in Figure 5.9 have been observed with other wire array samples as well, but these results are still preliminary due to complications arising from conformal deposition during the wire growth process. In some samples, conformally deposited Si (visible by SEM, data not shown) shows significant photoactivity even after all the wires have been removed. Thus, more detailed exploration of the influence of KOH etching on the photoelectrochemical properties of wire arrays will require samples known to have little or no conformally deposited Si at the base of the wires. Despite their preliminary nature, these results suggest that further improvements in the Si wire array performance at the same geometry will require changing to a different VLS catalyst that has a less deleterious effect on Si or devising an efficient gettering system to increase the purity of the wires produced.

5.4.5 Scanning Confocal Microscopy of Wire Arrays

It was shown above by both mechanical wire removal and chemical wire removal that that the n^+-Si substrate is not photoactive following wire growth. In order to provide more support for the dominance of the wires in the observed photoelectrochemical responses, scanning confocal microscopy experiments were undertaken to differentiate photoresponse from the wires and from the substrate. In brief, a long working distance confocal microscope objective was used to focus monochromatic light (650 nm) through a coverslip onto a liquid junction cell containing a wire array sample (Figure 5.10). In this case, the solvent used was propylene carbonate due to its lower vapor pressure, and a slightly higher concentration of Me_2FcBF_4 (10 mM) was used. A Pt wire was used as both the counter electrode and a pseudoreference. The focused laser spot was scanned

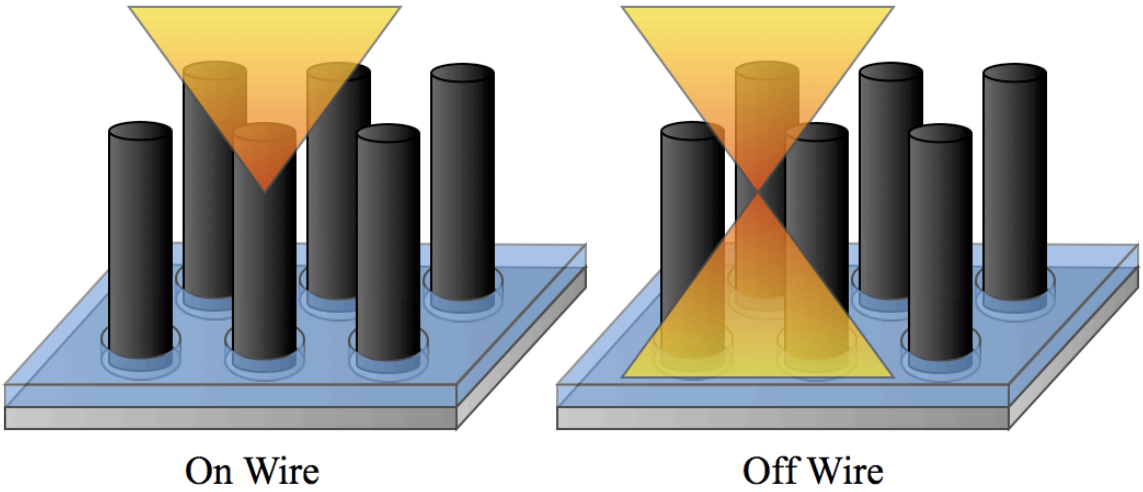

Figure 5.10. *Schematic of scanning confocal microscopy experiments. Si wires are shown growing vertically from the substrate through a thin oxide layer. When the focal point of the incident light is focused on a wire, most of the light should be absorbed by that wire. However, when the focal point is between wires, the defocused beam may intersect many neighboring wires, producing significant absorption.*

across the sample and the photocurrent was measured at each point with a chopper and a lock-in amplifier. In this way, an image can be constructed, with each pixel false colored to represent the measured photocurrent.

Figure 5.11 shows a false-color map of the photocurrent after scanning a wire array sample. The positions of the wires in the image are readily apparent as areas of increased photocurrent. Furthermore, the center-center distance between bright areas is commensurate with the value expected from the mask used, and the bright areas are arranged in a square array. Note, however that the wire diameter as measured by SEM is much smaller than that observed in the scanning microscopy experiments. As suggested by Figure 5.10, because of the tight focus of the laser spot from a confocal objective, it is likely that the beam broadens significantly both above and below the focal plane. Thus, even when the laser spot is not focused directly on a wire, there is expected to be significant absorption by nearby wires due to spreading of the beam. This also accounts

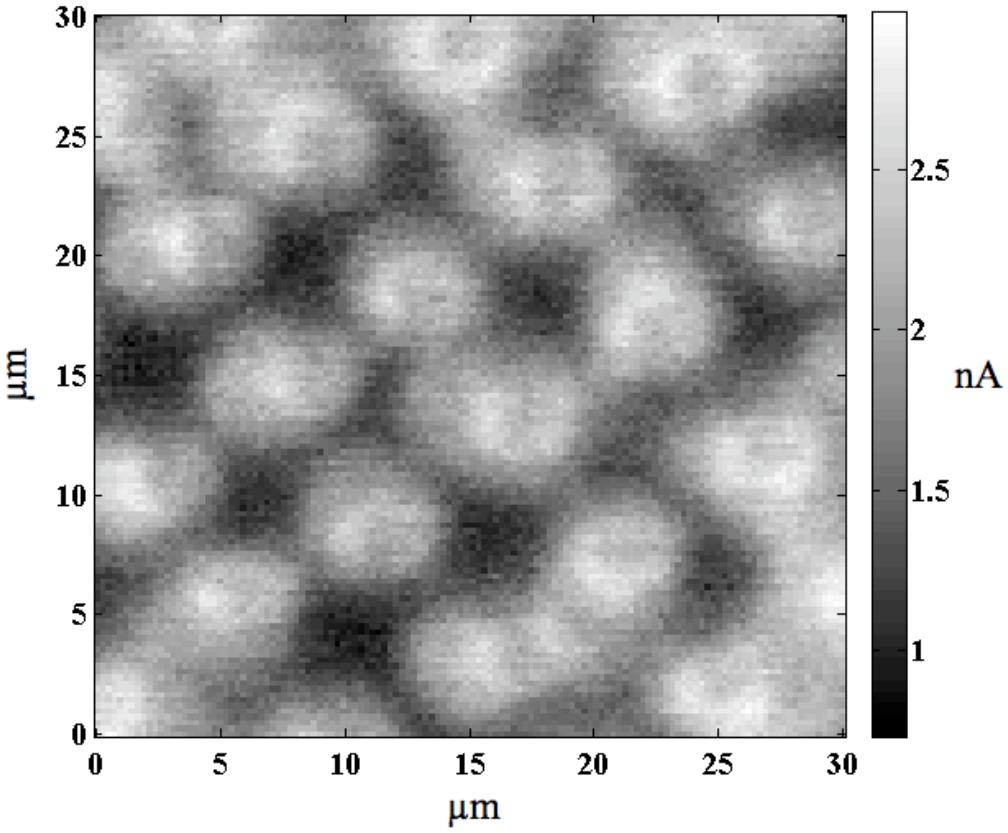

Figure 5.11. *False-color map of a wire array sample. The current scale is shown in nA, and the pixel positions have been scaled to match the approximate real distance traversed during the scan.*

for the significant photocurrent observed even in the darkest areas between rods (~0.75 nA). Thus, although the wires are clearly visible and more photoactive than the substrate, it is difficult to remove contributions from neighboring wires to see only the substrate. However, combined with measurements of the substrate following mechanical or chemical removal of wire arrays, these data strongly support that the observed photoelectrochemical properties described above are attributable to the CVD-grown Si wires rather than to the single crystalline substrate.

5.5 Conclusions

The Au-catalyzed, CVD-grown Si wire arrays examined in these studies show significantly improved efficiencies as compared with those presented in Chapter 4. In particular, the J_{sc} values were nearly an order of magnitude larger than those initially observed, and the fill factor values were improved as well. However, the observed V_{oc} was decreased relative to that observed in Chapter 4, possibly due to the same geometric factors that lead to an increased value of J_{sc}. However, there are likely to be other contributing factors to the lowered V_{oc}, such as changes in materials properties and doping levels. Despite decreases in V_{oc}, even the raw data collected in this study shows much improved efficiency as compared to the previously examined wire array samples. Correction of the raw data for concentration overpotential and solution series resistance losses further improves the fill factor, J_{sc}, and efficiency of these devices. In order to verify the validity of these corrections, extensive studies were performed using photoelectrochemical cells having an increased [Me_2Fc^+]. These studies showed that the concentration overpotential correction calculated from the measured limiting currents correctly accounts for the experimentally observed improvement when moving to a system that is not as limited by mass transport. Therefore, the reported efficiency of about 1.5% is expected to reflect the performance that these wire arrays would exhibit in a system in which both concentration overpotential and series resistance losses have been minimized (e.g., a thin layer cell). Attempts to improve the energy conversion efficiency of the wires by removing the outer, Au-rich layer have so far yielded only decreases in wire performance, indicating that further steps will need to be taken to replace Au as the

VLS catalyst or to remove it from the wires after growth. Finally, the negligible contribution of the n^+-Si substrate to the observed photoelectrochemical behavior has been demonstrated by removal of the wires both chemically and mechanically as well as by scanning confocal microscopy experiments.

5.6 References

1. Maiolo, J. R.; Kayes, B. M.; Filler, M. A.; Putnam, M. C.; Kelzenberg, M. D.; Atwater, H. A.; Lewis, N. S. *J. Am. Chem. Soc.* **2007**, *129*, 12346-12347.
2. Kayes, B. M.; Atwater, H. A.; Lewis, N. S. *J. Appl. Phys.* **2005**, *97*, 114302.
3. Wagner, R. S.; Ellis, W. C. *Transactions of the Metallurgical Society of Aime* **1965**, *233*, 1053-&.
4. Wu, Y.; Cui, Y.; Huynh, L.; Barrelet, C. J.; Bell, D. C.; Lieber, C. M. *Nano Lett.* **2004**, *4*, 433-436.
5. Cui, Y.; Lauhon, L. J.; Gudiksen, M. S.; Wang, J. F.; Lieber, C. M. *Appl. Phys. Lett.* **2001**, *78*, 2214-2216.
6. Lombardi, I.; Hochbaum, A. I.; Yang, P.; Carraro, C.; Maboudian, R. *Chem. Mat.* **2006**, *18*, 988-991.
7. Hochbaum, A. I.; Fan, R.; He, R. R.; Yang, P. D. *Nano Lett.* **2005**, *5*, 457-460.
8. Law, M.; Goldberger, J.; Yang, P. D. *Annual Review of Materials Research* **2004**, *34*, 83-122.
9. Wu, Y. Y.; Yang, P. D. *J. Am. Chem. Soc.* **2001**, *123*, 3165-3166.
10. Hannon, J. B.; Kodambaka, S.; Ross, F. M.; Tromp, R. M. *Nature* **2006**, *440*, 69-71.
11. Kodambaka, S.; Hannon, J. B.; Tromp, R. M.; Ross, F. M. *Nano Lett.* **2006**, *6*, 1292-1296.
12. Kodambaka, S.; Tersoff, J.; Reuter, M. C.; Ross, F. M. *Phys. Rev. Lett.* **2006**, *96*.
13. Lew, K. K.; Pan, L.; Bogart, T. E.; Dilts, S. M.; Dickey, E. C.; Redwing, J. M.; Wang, Y. F.; Cabassi, M.; Mayer, T. S.; Novak, S. W. *Appl. Phys. Lett.* **2004**, *85*, 3101-3103.
14. Lew, K. K.; Reuther, C.; Carim, A. H.; Redwing, J. M.; Martin, B. R. *J. Vac. Sci. Technol. B* **2002**, *20*, 389-392.
15. Wang, Y. F.; Lew, K. K.; Ho, T. T.; Pan, L.; Novak, S. W.; Dickey, E. C.; Redwing, J. M.; Mayer, T. S. *Nano Lett.* **2005**, *5*, 2139-2143.
16. Fang, H.; Wu, Y.; Zhao, J.; Zhu, J. *Nanotechnology (UK)* **2006**, 3768-3768.
17. Huang, Z. P.; Fang, H.; Zhu, J. *Adv. Mater.* **2007**, *19*, 744-+.

18. Peng, K. Q.; Wu, Y.; Fang, H.; Zhong, X. Y.; Xu, Y.; Zhu, J. *Angew. Chem.-Int. Edit.* **2005**, *44*, 2737-2742.

19. Z. Huang, H. F. *Adv. Mater.* **2007**, *19*, 744-748.

20. Gowrishankar, V.; Miller, N.; McGehee, M. D.; Misner, M. J.; Ryu, D. Y.; Russell, T. P.; Drockenmuller, E.; Hawker, C. J. *Thin Solid Films* **2006**, *513*, 289-294.

21. Kayes, B. M.; Filler, M. A.; Putnam, M. C.; Kelzenberg, M. D.; Lewis, N. S.; Atwater, H. A. *Appl. Phys. Lett.* **2007**, *91*, 103110.

22. Plass, K. E.; Filler, M. A.; Spurgeon, J. M.; Kayes, B. M.; Maldonado, S.; Brunschwig, B. S.; Atwater, H. A.; Lewis, N. S. *Adv. Mater.* **2009**, *21*, 325-328.

23. Spurgeon, J. M.; Plass, K. E.; Kayes, B. M.; Brunschwig, B. S.; Atwater, H. A.; Lewis, N. S. *Appl. Phys. Lett.* **2008**, *93*.

24. Kelzenberg, M. D.; Turner-Evans, D. B.; Kayes, B. M.; Filler, M. A.; Putnam, M. C.; Lewis, N. S.; Atwater, H. A. *Nano Lett.* **2008**, *8*, 710-714.

25. Sze, S. M. *Physics of Semiconductor Devices*; 2nd ed.; John Wiley & Sons: New York, 1981.

26. Bullis, W. M.; Strieter, F. J. *J. Appl. Phys.* **1968**, *39*, 314-&.

27. Struthers, J. D. *J. Appl. Phys.* **1956**, *27*, 1560-1560.

28. Wilcox, W. R.; Lachapelle, T. J. *J. Appl. Phys.* **1964**, *35*, 240-&.

29. Putnam, M. C.; Filler, M. A.; Kayes, B. M.; Kelzenberg, M. D.; Guan, Y. B.; Lewis, N. S.; Eiler, J. M.; Atwater, H. A. *Nano Lett.* **2008**, *8*, 3109-3113.

30. Lewis, N. S. *J. Electrochem. Soc.* **1984**, *131*, 2496-2503.

31. Rosenbluth, M. L.; Lewis, N. S. *J. Phys. Chem.* **1989**, *93*, 3735-3740.

32. Rosenbluth, M. L.; Lewis, N. S. *J. Am. Chem. Soc.* **1986**, *108*, 4689-4695.

33. Forbes, M. D. E.; Lewis, N. S. *J. Am. Chem. Soc.* **1990**, *112*, 3682-3683.

34. Kenyon, C. N.; Tan, M. X.; Kruger, O.; Lewis, N. S. *J. Phys. Chem. B* **1997**, *101*, 2850-2860.

35. Kruger, O.; Kenyon, C. N.; Tan, M. X.; Lewis, N. S. *J. Phys. Chem. B* **1997**, *101*, 2840-2849.

36. Tan, M. X.; Kenyon, C. N.; Kruger, O.; Lewis, N. S. *J. Phys. Chem. B* **1997**, *101*, 2830-2839.

37. Tan, M. X.; Kenyon, C. N.; Lewis, N. S. *J. Phys. Chem.* **1994**, *98*, 4959-4962.

38. Rosenbluth, M. L.; Lieber, C. M.; Lewis, N. S. *Appl. Phys. Lett.* **1984**, *45*, 423-425.

39. Gibbons, J. F.; Cogan, G. W.; Gronet, C. M.; Lewis, N. S. *Appl. Phys. Lett.* **1984**, *45*, 1095-1097.

40. Gronet, C. M.; Lewis, N. S.; Cogan, G. W.; Gibbons, J. F. *Proc. Natl. Acad. Sci.* **1983**, *80*, 1152-1156.

41. Cogan, G. W.; Gronet, C. M.; Gibbons, J. F.; Lewis, N. S. *Appl. Phys. Lett.* **1984**, *44*, 539-541.

42. Gstrein, F.; Michalak, D. J.; Royea, W. J.; Lewis, N. S. *J. Phys. Chem. B* **2002**, *106*, 2950-2961.

43. Groner, M. D.; Koval, C. A. *J. Electroanal. Chem.* **2001**, *498*, 201-208.

44. Beermann, N.; Vayssieres, L.; Lindquist, S. E.; Hagfeldt, A. *J. Electrochem. Soc.* **2000**, *147*, 2456-2461.

45. Baxter, J. B.; Aydil, E. S. *Appl. Phys. Lett.* **2005**, *86*.

46. Law, M.; Greene, L. E.; Johnson, J. C.; Saykally, R.; Yang, P. D. *Nat. Mater.* **2005**, *4*, 455-459.

47. Law, M.; Greene, L. E.; Radenovic, A.; Kuykendall, T.; Liphardt, J.; Yang, P. D. *J. Phys. Chem. B* **2006**, *110*, 22652-22663.

48. Gur, I.; Fromer, N. A.; Geier, M. L.; Alivisatos, A. P. *Science* **2005**, *310*, 462-465.

49. Takanezawa, K.; Hirota, K.; Wei, Q. S.; Tajima, K.; Hashimoto, K. *J. Phys. Chem. C* **2007**, *111*, 7218-7223.

50. Wei, Q. S.; Hirota, K.; Tajima, K.; Hashimoto, K. *Chem. Mat.* **2006**, *18*, 5080-5087.

51. Peng, K. Q.; Xu, Y.; Wu, Y.; Yan, Y. J.; Lee, S. T.; Zhu, J. *Small* **2005**, *1*, 1062-1067.

52. Goodey, A. P.; Eichfeld, S. M.; Lew, K. K.; Redwing, J. M.; Mallouk, T. E. *J. Am. Chem. Soc.* **2007**, *129*, 12344-+.

53. Dalchiele, E. A.; Martín, F.; Leinen, D.; Marotti, R. E.; Ramos-Barrado, J. R. *J. Electrochem. Soc.* **2009**, *156*, K77-K81.

54. Stelzner, T.; Pietsch, M.; Andra, G.; Falk, F.; Ose, E.; Christiansen, S. *Nanotechnology (UK)* **2008**, *19*.

55. Tsakalakos, L.; Balch, J.; Fronheiser, J.; Korevaar, B. A.; Sulima, O.; Rand, J. *Appl. Phys. Lett.* **2007**, *91*.

56. Garnett, E. C.; Yang, P. D. *J. Am. Chem. Soc.* **2008**, *130*, 9224-+.

57. Lewis, N. S.; Gronet, C. M. *Appl. Phys. Lett.* **1983**, *43*, 115-117.

58. Fajardo, A. M.; Lewis, N. S. *J. Phys. Chem. B* **1997**, *101*, 11136-11151.

59. Lewis, N. S.; Rosenbluth, M. L. In *Photocatalysis: Fundamentals and Applications*; Serpone, N., Pelizzetti, E., Eds.; Wiley Interscience: New York, 1989, p 45-121.

60. ASTM Standard G173, 2003e1, "Standard Tables for Reference Solar Spectral Irradiances: Direct Normal and Hemispherical on 37º Tilted Surface," ASTM International, West Conshohocken, PA, 2003, DOI: 10.1520/G0173-03E01.

61. Maiolo, J. R.; Atwater, H. A.; Lewis, N. S. *J. Phys. Chem. C* **2008**, *112*, 6194-6201.

62. Lehmann, V. *Electrochemistry of Silicon: Instrumentation, Science, Materials and Applications*; Wiley-VCH, 2002.